

541588

# **Comparison of Shortwave Cloud Radiative Forcing Derived from ARM SGP Surface and GOES-8 Satellite Measurements During ARESE I and ARESE II**

*A.D. Rapp, D.R. Doelling, M.M. Khaiyer  
Analytical Services & Materials, Inc.  
Hampton, VA*

*P. Minnis, W.L. Smith, Jr., L. Nguyen, M.P. Haeffelin  
NASA Langley Research Center  
Hampton, VA*

*F.P.J. Valero  
Scripps Institution of Oceanography  
La Jolla, CA*

*S. Asano  
Tohoku University  
Japan*

Eleventh ARM Science Team Meeting Proceedings  
Atlanta, Georgia  
March 19-23, 2001

# Comparison of Shortwave Cloud Radiative Forcing Derived from ARM SGP Surface and GOES-8 Satellite Measurements During ARESE I and ARESE II

*A.D. Rapp, D.R. Doelling, M.M. Khaiyer  
Analytical Services & Materials, Inc.  
Hampton, VA*

*P. Minnis, W.L. Smith, Jr., L. Nguyen, M.P. Haeffelin  
NASA Langley Research Center  
Hampton, VA*

*F.P.J. Valero  
Scripps Institution of Oceanography  
La Jolla, CA*

*S. Asano  
Tohoku University  
Japan*

## Introduction

One of the objectives of the ARM Enhanced Shortwave Experiment (ARESE) is to investigate the absorption of solar radiation by clouds over the ARM Southern Great Plains central facility. A variety of techniques employing various combinations of surface, aircraft, and satellite data have been used to estimate the absorption empirically. During ARESE-I conducted during fall 1995, conflicting results were produced from different analyses of the combined datasets leading to the need for a more controlled experiment. ARESE-II was conducted during spring 2000. Improved calibrations, different sampling strategies, and broadband satellite data were all available to minimize some of the sources of uncertainty in the data. In this paper, cloud absorption or its parametric surrogates (e.g., Cess et al. 1995) are derived from collocated and coincident surface and satellite radiometer data from both ARESE-I and ARESE-II using the latest satellite and surface instrument calibrations.

## Data

### *Satellite*

Half-hourly visible (VIS; 0.65  $\mu\text{m}$ ) data from the eighth Geostationary Operational Environmental Satellite (GOES-8) were used to compute the top-of-atmosphere (TOA) albedos in the analyses for both ARESE-I and ARESE-II. The GOES-8 visible channel was calibrated against Visible Infrared Scanner (VIRS) data from 1998 - 2000 to determine visible radiances (Minnis et al., 2001). This GOES-8 calibration was extrapolated back to the ARESE I time period. Excellent agreement between GOES-8 data and the self-calibrating ATSR-2 satellite data supports the use of this extrapolation. The visible radiances were converted to visible albedo,  $\alpha_v$ , as in Minnis et al. (1995). GOES-8 broadband shortwave (SW; 0.2 - 5.0  $\mu\text{m}$ ) albedo,  $\alpha_b$ , was calculated using two different conversion methods for

comparison. The first, derived from correlations of GOES-6 narrowband data and Earth Radiation Budget Satellite (ERBS) broadband data during October 1986, is represented by

$$\alpha_b = 0.0571 + 0.7198\alpha_v - 0.0287\alpha_v^2 + 0.0523\ln(1/\mu_0). \quad [1]$$

The second, based on correlations of GOES-8 narrowband data and Clouds and the Earth's Radiant Energy System (CERES) broadband data during March 2000, is

$$\alpha_b = 0.0406 + 0.8648\alpha_v - 0.10655\alpha_v^2 + 0.00865\ln(1/\mu_0), \quad [2]$$

where  $\mu_0$  is the cosine of the solar zenith angle.

### *Surface*

Four different radiometer platforms from the central facility were utilized for the surface flux analyses during ARESE-II. The Solar Infrared Radiation Station (SIRS) platform consists of both up- and down-looking radiometers, while the Total Solar Broadband Radiometer (TSBR; Valero et al. 1997), Kipp and Zonen CM-21, and Haeffelin PSP (Haeffelin et al. 2001a) consist of up-looking radiometers only. For the ARESE-I, only the SIROS (the SIROS platform was replaced by SIRS in 1997) and TSBR platforms were available. All of the surface broadband shortwave flux measurements were averaged at half-hour intervals centered on the GOES-8 satellite image times.

## **Methodology**

These data were analyzed with the methods of Cess et al. (1995). The clear-sky broadband measurements were identified and fit using linear regression for both the surface and satellite data. The differences between the actual measurement and the clear-sky fit lines are the instantaneous TOA and surface SW cloud forcings. At the TOA, the SW cloud forcing is

$$TCRF = \Sigma \{E_0(\delta)\mu_0(\alpha_{clr} - \alpha_{cld})\} \quad [3]$$

where  $E_0$  is the solar constant and  $\delta$  is the relative Earth-Sun distance. For the surface the SW cloud forcing is

$$SCRF = \Sigma \{M_{clr} - M_{cld}\} \quad [4]$$

where  $M$  is either the net downward shortwave flux or surface insolation. The forcing ratio,  $R$ , is defined as the ratio of the surface-to-TOA SW cloud forcing,

$$R = SCRF/TCRF. \quad [5]$$

An alternate approach to quantify cloud forcing and absorption is to determine the albedo-transmission slope,  $\beta$  (Cess et al., 1995), where

$$\beta = -d\alpha_b/d(\text{sfc insolation/toa insolation}). \quad [6]$$

A simple, single fit to the albedo and the insolation ratio data often does not yield a line that intersects the main clusters of data. To achieve a more representative fit, an average linear fit was computed by determining the slopes for the fits using one data set and then the other as the dependent variable. Such an approach is justified because the one of the greatest uncertainties in the matched data is due to mismatching the temporal average surface data with the spatially averaged satellite data. This approach yields lines that intersect the main data clusters.

By integrating [6], the forcing ratio can be related to  $\beta$  by

$$R = SCRF/TCRF = (1 - \alpha_s) / \beta, \quad [7]$$

where  $\alpha_s$  is the surface albedo. Using the calculated values of R and  $\beta$  and solving for surface albedo yields surface albedos that make physical sense and agree with those calculated from the SIRS platform if the average fit method for  $\beta$  is used. The simple the x-y fit method, however, produces surface albedo values that are much greater than the observations.

The ARESE-II data were divided into 3 different categories: all coincident GOES-8 and surface instrument points, all coincident GOES-8 and surface instrument points that are also coincident with ARM-UAV flights, and all coincident CERES and surface instrument points.

## Model Calculations

For comparison with the actual measurements, results for ARESE II were generated using a modified Fu-Liou model (FL; Fu and Liou, 1992, 1993). The FL model was used to compute the surface and TOA fluxes for the identified clear-sky cases utilizing the nearest sounding from the central facility, MFRSR aerosol optical depths, and SIRS half-hour averaged surface albedo as inputs. To model the cloudy scenes, four cases from ARESE II were chosen: three stratus (03/03,03/21,03/09) and one cirrus (03/09). Corresponding sounding data were used, as well as cloud optical depth and particle size derived from GOES-8 cloud products (Minnis et al. 2001). A comparison of the GOES-8 and FL TOA fluxes can be seen in Figure 1.

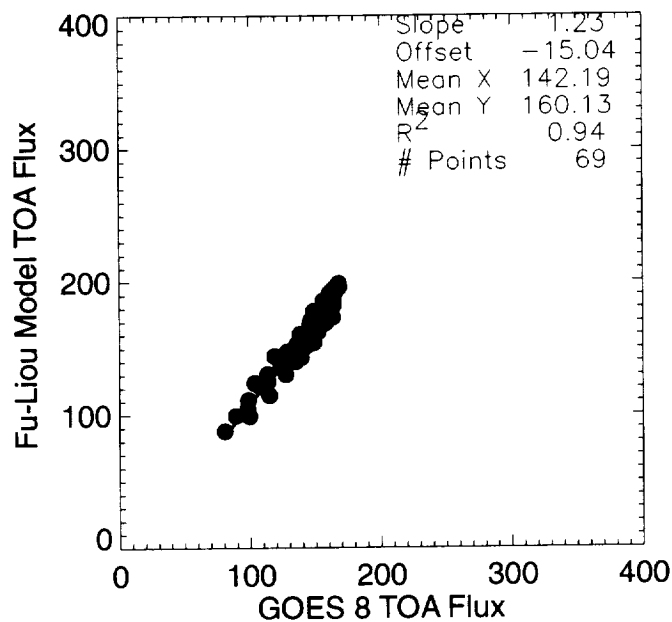


Figure 1. GOES 8 TOA flux vs. Fu-Liou model TOA flux.

## Results

The cloud forcing ratio as calculated from coincident GOES-8 using the ERBS narrowband-to-broadband formula and SIRS surface data for ARESE-I and ARESE-II are shown in Figs. 2 and 3, respectively. Figure 2 shows an  $R$  value for ARESE-I that is less than that for ARESE-II in Fig. 3. The Fu-Liou model results compare well with the ARESE-II results, yielding the same value of 1.10 for  $R$ . The difference between the ARESE-I and ARESE-II values could be due to the narrowband calibration, uncertainties in the surface measurements, or to differences in the cloud and surface properties. The SIROS data may underestimate the downwelling fluxes up to  $30 \text{ Wm}^{-2}$  (Gulbrandsen 1978; Cess et al. 1999) in very clear conditions due to thermal effects that introduce a variable offset (Haeffelin et al. 2001b). Applying a thermal correction to these surface data should bring the forcing ratios in closer agreement for ARESE I and ARESE II.

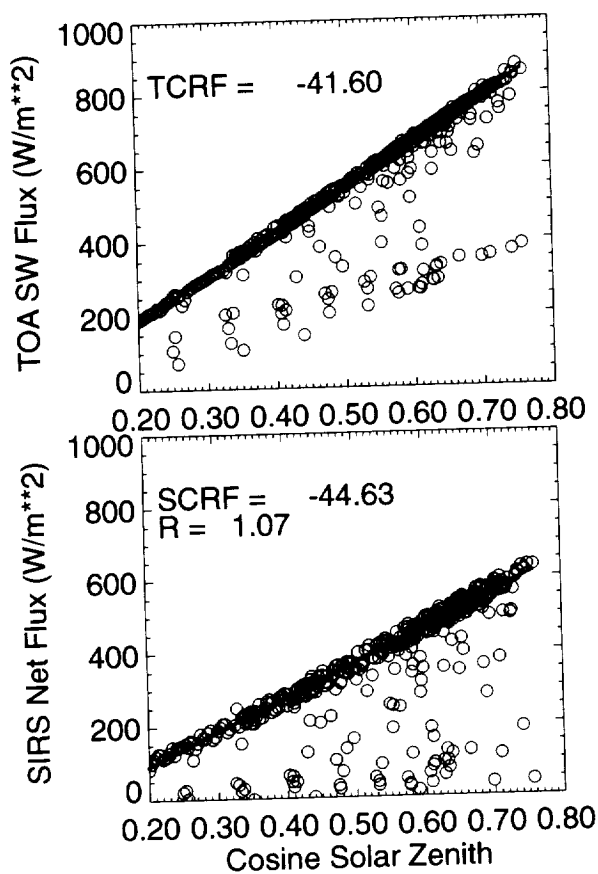


Figure 2. ARESE I TOA and surface cloud radiative forcing and forcing ratio.

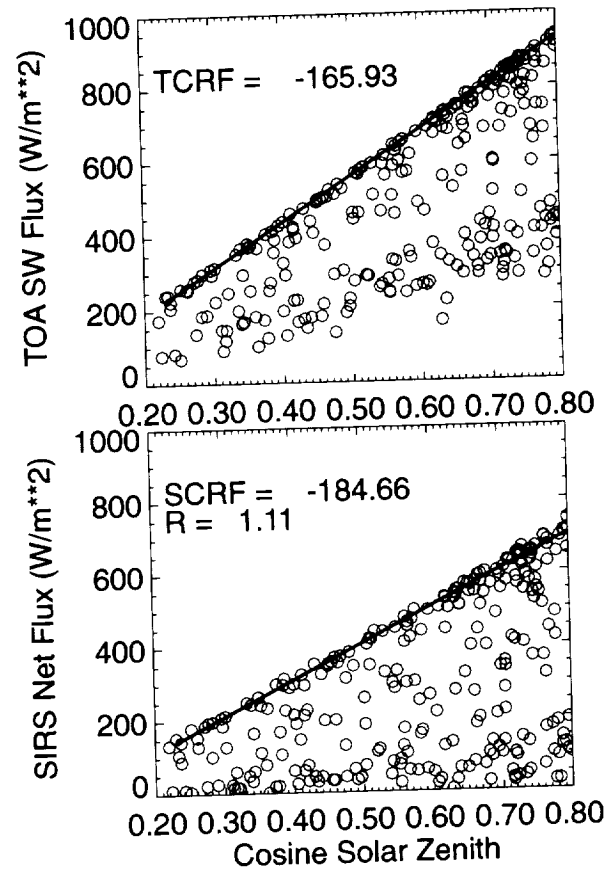


Figure 3. ARESE II TOA and surface cloud radiative forcing and forcing ratio.

The values for  $\beta$  using the average fit method for both experiments and both GOES-8 and CERES satellite data show very good agreement, with values ranging from 0.71 to 0.74 as seen in Figs. 4-7. The FL model results (Fig. 7) yield a  $\beta$  value very near that calculated from the ARESE I and II measurements. Note that both the x-y and y-x fits yield the same slopes for the model data because there are no uncertainties in matching the TOA and surface values.

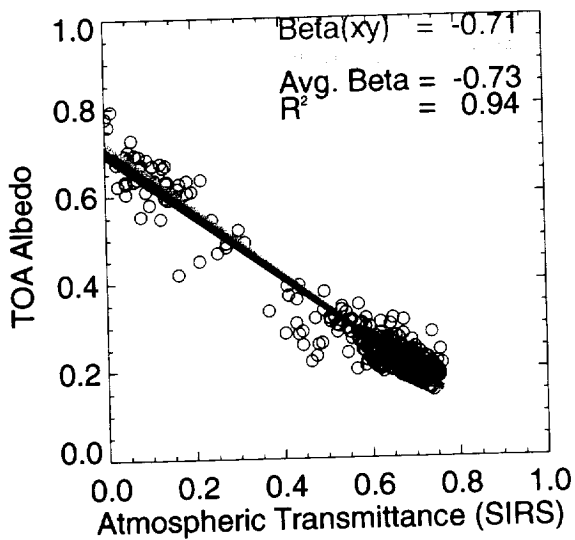


Figure 4. ARESE I albedo/transmission slope using GOES satellite and SIRS surface data.

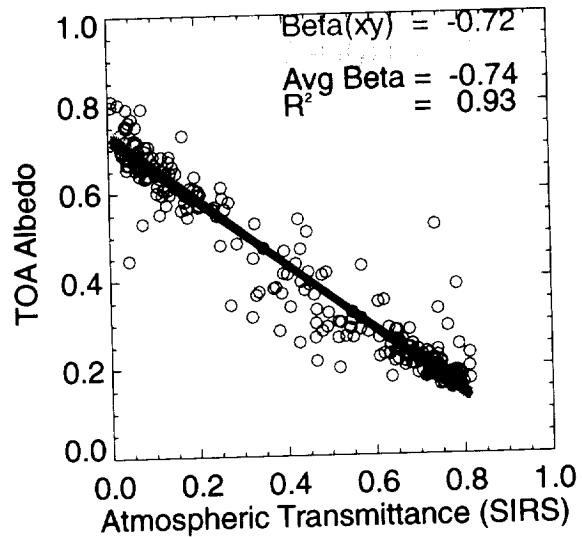


Figure 5. ARESE II albedo/transmission slope using GOES satellite and SIRS surface data.

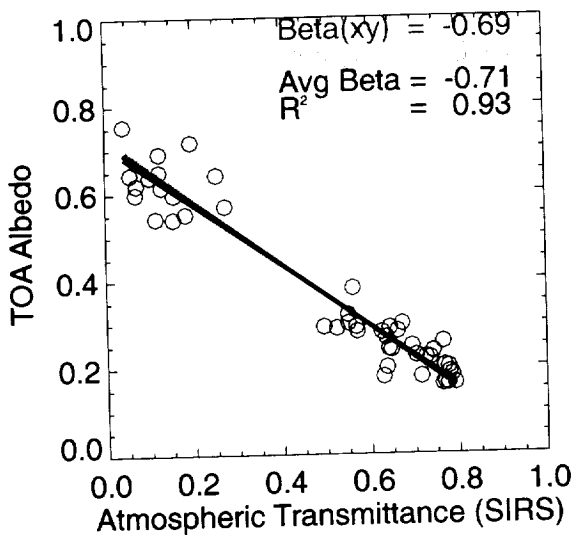


Figure 6. ARESE II albedo/transmission slope using CERES satellite and SIRS surface data.

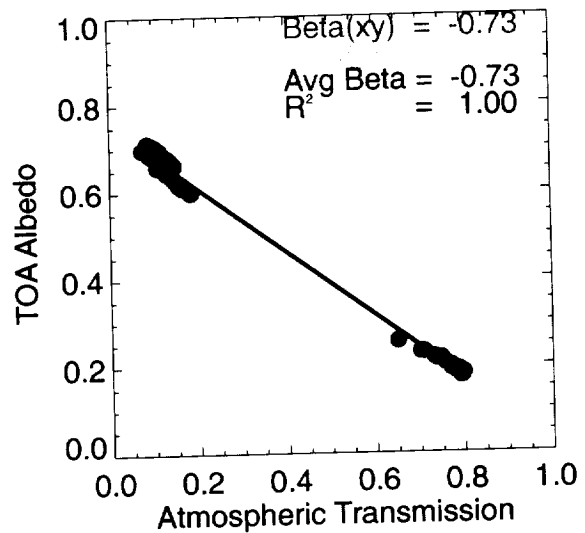


Figure 7. Fu-Liou Model albedo/transmission slope for ARESE II simulation.

Table 1 depicts the mean values of the absorption parameters found for ARESE-I and ARESE-II using the three subsets of data, up to four different surface instruments, two satellite datasets, and two different narrowband-to-broadband conversions. From the table we see that the values for  $R$  and  $\beta$  during ARESE I are less than those for ARESE II, as well as model predictions. Although the narrowband-to-broadband conversion is still an issue, it seems to make only a minor difference in the absorption calculations, with the ERBE narrowband-to-broadband conversion typically showing similar results for  $\beta$  values and only slightly higher values for  $R$ . The mean parameter values in Table 1 for ARESE-II using the CERES data are in excellent agreement with the FL results. The GOES-8 results for ARESE-II are also close, but are biased by 5%. This bias may be a result of inaccuracies in the clear-sky albedos for GOES-8. Overall, the actual results are much closer to the model calculations than previous studies have shown suggesting that there is no anomalous SW absorption for these cases.

Table 1. Mean absorption parameters for ARESE I and ARESE II.

NB-BB Conversion	$R_{insol}$		$R_{net}$		$\beta$		$(1-\alpha)/\beta$	
	ERBE	CERES	ERBE	CERES	ERBE	CERES	ERBE	CERES
ARESE I, GOES	1.38	1.36	1.07	1.00	0.72	0.73	1.07	1.05
ARESE II, GOES	1.38	1.31	1.11	1.07	0.75	0.75	1.08	1.08
ARESE II, CERES	1.38		1.16		0.71		1.14	
Fu-Liou Model	1.38		1.10		0.73		1.13	

## Concluding Remarks

The preliminary results shown here support the accuracy of the Fu-Liou model for computing atmospheric absorption and surface radiation. Other model formulations were not tested, so the conclusions are not universally applicable. The ARESE-I results differ substantially from those computed with the earlier GOES-8 calibration as a result of using the average linear fit and a new narrowband calibration for GOES-8. Instead of anomalous absorption, the satellite measurements, when combined with the surface observations, now yield less absorption than expected. However, correction of the instrument errors could bring the ARESE-I and ARESE-II results into even closer agreement. The results found here, along with those from aircraft data taken during ARESE-II should help improve our understanding of absorption of shortwave radiation in the atmosphere.

## References

- Cess, R.D., X. Jing, T. Qian, and M. Sun, 1999: Validation strategies applied to the measurement of total, direct and diffuse shortwave radiation at the surface. *J. Geophys. Res.*,
- Cess, R.D., M.H. Zhang, P. Minnis, L. Corsetti, E.F. Dutton, B.W. Forgan, D.P. Garber, W.L. Gates, J.J. Hack, E.F. Harrison, X. Jing, J.T. Kiehl, C.N. Long, J.-J. Morcrette, G.L. Potter, V. Ramanathan, B. Subasilar, C.H. Whitlock, D.F. Young, Y. Zhou, 1995: Absorption of solar radiation by clouds: observations versus models. *Science*, **267**, 496-499.
- Fu, Q., and K.-N. Liou, 1992: On the correlated k-distribution method for radiative transfer in nonhomogenous atmospheres. *J. Atmos. Sci.*, **49**, 2139-2156.

**CERES Validation Parameters:**

**Top-of-Atmosphere shortwave (SW), longwave (LW)  
and Window (WN) channel fluxes**

**Time/Space Scale:**

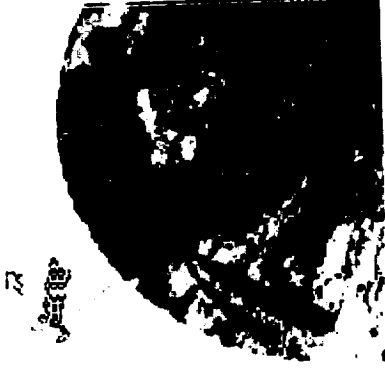
**Tropical (TRMM), Global (Terra and Aqua), 1° regional mean,  
instantaneous**

**Accuracy Goal:**

**1 W m<sup>-2</sup> global monthly mean  
10 W m<sup>-2</sup> instantaneous**

**Spacecraft Missions:**

**TRMM (11/97 launch), Terra(12/99 launch), Aqua (early 2002 launch)**



**LOCATION OF CAR BRDF DURING CLAMS-2001**  
**July 9–August 2**

Date	UW Flt. #	Target	Latitude	Longitude	Time (UTC)	Satellite/other airplanes	Comments
July 10	1870	Chesapeake Lighthouse	36.94	-75.70	18:04-18:20	Terra, Cessna-210, OV-10	Good
		Chesapeake Lighthouse	37.18	-75.72	21:42-21:57		Some cirrus contamination
July 12	1871	Chesapeake Lighthouse	36.95	-75.62	12:18-12:25	Proteaus, ER-2, Cessna-210, OV-10	Heavy Cloud contamination
July 14	1872	Chesapeake Lighthouse	36.94	-75.66	15:55-16:18	Proteaus, Cessna-210, OV-10	Some cumulus contamination
July 16	1873	Buoy 44001	35.98	-73.99	17:56-18:14	Proteaus, Cessna-210, OV-10	cirrus contamination and data corruption
July 17	1874	Chesapeake Lighthouse	36.95	-75.68	16:46-17:08	Terra, Proteaus, LEAR, ER-2, Cessna-210, OV-10	Good
		Dismal Swamp	36.54	-76.46	17:27-17:35		cirro-cumulus contamination
July 23	1875	Buoy 44009	37.83	-74.34	15:00-15:19		Good
July 26	1878	Buoy 44014	36.46	-74.74	17:48-18:04	Terra, Proteaus, ER-2, OV-10	Good
July 30	1879	Chesapeake Lighthouse	36.88	-75.77	16:45-16:54	Terra, Proteaus, ER-2, OV-10	Heavy Cloud contamination
		Buoy 44014	36.90	-74.55	18:17-18:27		Some cumulus contamination
		Chesapeake Lighthouse	37.13	-75.59	19:05-19:20		Good
July 31	1880	Buoy 44004	38.56	-70.61	16:52-17:06	Terra, Proteaus, ER-2, OV-10	Good
		Dismal Swamp	36.55	-76.43	18:55-19:15		Good
August 2	1882	Chesapeake Lighthouse	37.04	-75.70	20:01-20:19	Terra, ER-2, OV-10	Good

**KEY**

UW - University of Washington

- Fu, Q., and K.-N. Liou, 1993: Parameterization of the radiative properties of cirrus clouds. *J. Atmos. Sci.*, **50**, 2008-2025.
- Gulbrandsen, A., 1978: On the use of pyranometers in the study of spectral solar radiation and atmospheric aerosols. *J. Appl. Meteorol.*, **17**, 899-904.
- Haeffelin, M., B. C. Dominquez, C. K. Rutledge, and S. Kato, 2001a: Improved measurements of the diffuse and global solar irradiances at the surface of the Earth. *Proc. 11<sup>th</sup> Arm Science Team Meeting*, Atlanta, GA, March 19-23.
- Haeffelin, M., S. Kato, A. M. Smith, C. K. Rutledge, T. P. Charlock, and J. R. Mahan, 2001b: Determination of the thermal offset of the Eppley precision spectral pyranometer. *Appl. Opt.*, **40**, 472-484.
- Minnis, P., W.L. Smith, Jr., D.P. Garber, J.K. Ayers, and D.R. Doelling, 1995: Cloud properties derived from GOES-7 for the spring 1994 ARM Intensive Observing Period using Version 1.0.0 of the ARM Satellite Data Analysis Program. *NASA RP 1366*, August, 59 pp.
- Minnis, P., L. Nguyen, D. R. Doelling, D. F. Young, and W. F. Miller, 2001: Rapid calibration of Operational and research meteorological satellite imagers, Part I: Use of the TRMM VIRS or ERS-2 ATSR-2 as a reference. Submitted to *J. Atmos. Oceanic Technol.*
- Minnis, P., W. L. Smith, Jr., and D. F. Young, 2001: Cloud macro- and microphysical properties derived from GOES over the ARM SGP domain. *Proc. 11<sup>th</sup> Arm Science Team Meeting*, Atlanta, GA, March 19-23.
- Valero, F. P. J., R. D. Cess, M. Zhang, S. K. Pope, A. Bucholtz, B. C. Bush, and J. Vitko, Jr., Absorption of solar radiation by clouds: Interpretations of collocated measurements. *J. Geophys. Res.*, **102**, 29,917-29,927, 1997.

## **Acknowledgements**

This research was supported by the Environmental Sciences Division of U.S. Department of Energy Interagency Agreement DE-AI02-97ER62341 under the ARM program.

Special thanks to Francisco P.J. Valero, Martial Haeffelin, and Shoji Asano for use of their respective radiometer datasets.